A Hybrid Cloud Regime Methodology Used to Evaluate Southern Ocean Cloud and Shortwave Radiation Errors in ACCESS

SHANNON MASON AND JENNIFER K. FLETCHER

School of Earth, Atmosphere and Environment, Monash University, Clayton, Victoria, Australia

JOHN M. HAYNES

Cooperative Institute for Research in the Atmosphere, Colorado State University, Fort Collins, Colorado

CHARMAINE FRANKLIN

Oceans and Atmosphere Flagship, Commonwealth Scientific and Industrial Research Organization, Aspendale, Victoria, Australia

ALAIN PROTAT

Centre for Australian Weather and Climate Research, Melbourne, Victoria, Australia

CHRISTIAN JAKOB

School of Earth, Atmosphere and Environment, Monash University, Clayton, and Australian Research Council Centre of Excellence for Climate System Science, Melbourne, Victoria, Australia

(Manuscript received 11 December 2014, in final form 19 April 2015)

ABSTRACT

A deficit of shortwave cloud forcing over the Southern Ocean is persistent in many global climate models. Cloud regimes have been widely used in model evaluation studies to make a process-oriented diagnosis of cloud parameterization errors, but cloud regimes have some limitations in resolving both observed and simulated cloud behavior. A hybrid methodology is developed for identifying cloud regimes from observed and simulated cloud simultaneously.

Through this methodology, 11 hybrid cloud regimes are identified in the ACCESS1.3 model for the high-latitude Southern Ocean. The hybrid cloud regimes resolve the features of observed cloud and characterize cloud errors in the model. The simulated properties of the hybrid cloud regimes, and their occurrence over the Southern Ocean and in the context of extratropical cyclones, are evaluated, and their contributions to the shortwave radiation errors are quantified.

Three errors are identified: an overall deficit of cloud fraction, a tendency toward optically thin low and midtopped cloud, and an absence of a shallow frontal-type cloud at high latitudes and in the warm fronts of extratropical cyclones.

To demonstrate the utility of the hybrid cloud regimes for the evaluation of changes to the model, the effects of selected changes to the model microphysics are investigated.

1. Introduction

The representation of clouds in global climate models (GCMs) is critical to modeling the earth's radiative energy budget, atmospheric circulation, and hydrological cycle, and many processes at smaller scales. Model evaluation studies consistently identify significant cloud errors (e.g., Gates et al. 1999; Zhang et al. 2005; Trenberth and Fasullo 2010) and—while GCMs are improving by some measures (Klein et al. 2013)—subsequent cloud feedbacks continue to be the greatest source of uncertainty in estimates of climate sensitivity (e.g., Cess et al. 1990, 1996; Colman 2003; Dufresne and Bony 2008). Many of the processes regulating cloud formation, composition, and behavior—and interactions with aerosols, radiation,

Corresponding author address: Shannon Mason, School of Earth, Atmosphere and Environment, 9 Rainforest Walk, Monash University, Wellington Road, Clayton VIC 3800, Australia.
E-mail: shannon.mason@monash.edu

DOI: 10.1175/JCLI-D-14-00846.1

and dynamics—occur at scales below the resolution of GCMs and must be parameterized. Errors related to parameterized cloud can compensate to match the bulk observations against which GCMs are tuned; for example, the recurring ''too few, too bright'' low cloud errors in many phase 3 of the Coupled Model Intercomparison Project (CMIP3) models nevertheless produced near-realistic radiative fluxes (Klein et al. 2013). To identify these compensating errors and to inform the improvement of parameterizations, there is a need for ''process oriented'' approaches to model evaluation (Stephens 2005; Jakob 2010).

To better understand cloud processes in observations, and to evaluate them in GCMs, we identify ''cloud regimes''—classes of cloud with common physical characteristics and atmospheric contexts—and quantify both the physical and microphysical properties of clouds and the atmospheric processes to which they correspond. Cloud regimes can be identified from dynamical or thermodynamical parameters (e.g., Bony and Dufresne 2005), or directly from observed cloud characteristics by using a clustering algorithm to identify repeating patterns of cloud properties (Jakob and Tselioudis 2003; Jakob et al. 2005). The latter cloud regimes, also called ''weather states,'' have proved useful in associating observed cloud properties with dynamical and thermodynamical conditions in the tropics (e.g., Rossow et al. 2005; Tan et al. 2013), extratropics (e.g., Gordon and Norris 2010; Haynes et al. 2011; Oreopoulos and Rossow 2011), and globally (e.g., Tselioudis et al. 2013; Oreopoulos et al. 2014). A challenge when using cloud regimes for model evaluation is to identify them in such a way that the representation of clouds in one or more GCMs can be compared against each other and satellite observations. There have been two approaches to identifying cloud regimes for model evaluation: In the first approach (Williams and Tselioudis 2007, hereafter WT07), cloud regimes are identified from the simulated cloud properties of each GCM using the same methodology as for satellite observations. This method has the advantage of using simulated cloud directly, so that the cloud regimes accurately represent the coherent structures of cloud properties in each model. A disadvantage is that each GCM engenders a new set of cloud regimes that may be very different from those observed; without a common set of cloud regimes, evaluation between model and observations is problematic. In the WT07 approach, if simulated cloud regimes are significantly different from observations, they may be subjectively grouped into ''principal'' cloud regimes for evaluation. Alternatively cloud regimes can be identified from satellite observations only and then simulated clouds are assigned to cloud regimes based on average cloud properties (Williams and Webb 2009, hereafter WW09). The WW09 method has the advantage of using a consistent set of observed cloud regimes for evaluation and model intercomparison, and this approach has been widely used in subsequent studies (e.g., Tsushima et al. 2013; Bodas-Salcedo et al. 2012, 2014). A disadvantage of the WW09 methodology is that the observed cloud regimes are not necessarily representative of the coherent structures of cloud properties in the models, so that the links between cloud properties and processes in the GCM are uncertain. In this paper we aim to extend these approaches by developing a hybrid methodology that retains the structures of both observed and simulated clouds. Hybrid cloud regimes are identified from observed and simulated cloud simultaneously, ensuring the retention of observed cloud regimes to which the model must be compared, while including the cloud structures peculiar to the model—and hence the errors we aim to explore.

We apply the hybrid cloud regime methodology to a significant cloud evaluation problem for many state-of-the-art models: the shortwave (SW) radiation biases in the high-latitude Southern Ocean (50°–65°S) during the austral summer [December–February (DJF)]. An excess of absorbed SW radiation in this region—associated with a deficit of cloud or cloud reflectivity—was identified in CMIP3 (Trenberth and Fasullo 2010), and persists in the CMIP5 models (Li et al. 2013). Evaluations of the Met Office (UKMO) model and other CMIP5 models using the WW09 methodology (Bodas-Salcedo et al. 2012, 2014) have attributed the radiation biases to low and midtopped cloud regimes, especially in the postfrontal and cold-air part of extratropical cyclones. Observational studies have shown that the high-latitude Southern Ocean is dominated by near-ubiquitous low cloud, much of which is assigned by passive satellite observations to midtopped cloud regimes (Haynes et al. 2011; Bodas-Salcedo et al. 2014). While WW09 identify a single midtopped cloud regime in the Southern Ocean, observational studies distinguish between two midtopped cloud regimes with distinct dynamical contexts and radiative properties (Haynes et al. 2011), and further evaluation of these midtopped cloud regimes at high latitudes has shown that the optically thicker midtopped cloud regime includes instances of both stratiform cloud under strongly subsiding conditions and shallow frontal-type clouds, which were associated with conditions resembling the warm conveyor belt in extratropical cyclones (Mason et al. 2014). Resolving these distinct cloud processes associated with midtopped cloud in observations and GCMs is a priority for an extended cloud regime methodology.

The GCM used in this study is the Australian Community Climate and Earth-System Simulator, version

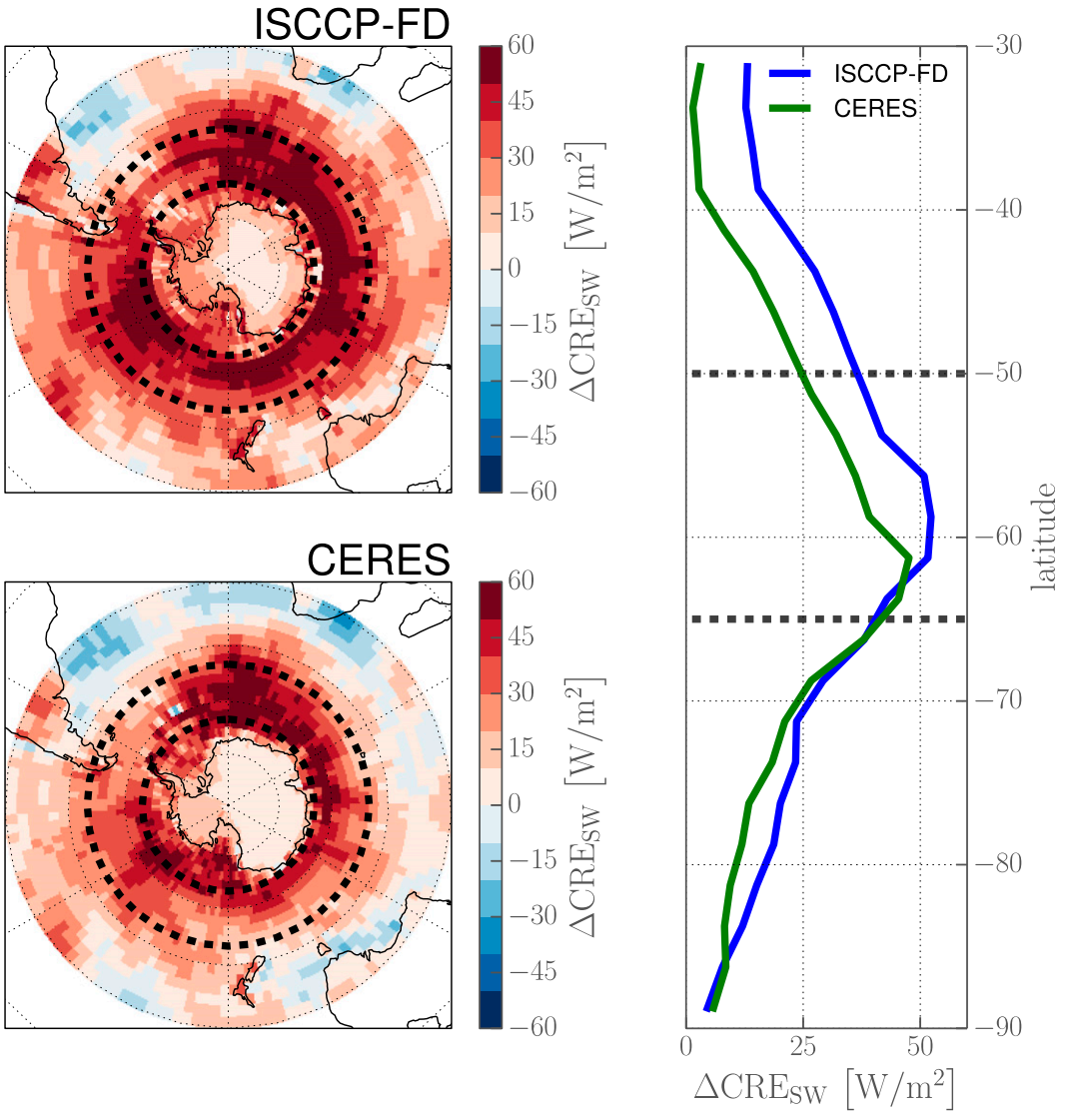

FIG. 1. Maps of the CRE_{SW} bias in ACCESS1.3 with respect to (top left) ISCCP-FD observations and (bottom left) CERES SYN1deg over the Southern Hemisphere extratropics, and (right) the zonal means of the same. The high-latitude Southern Ocean region taken as the area of interest for this study (50°–65°S) is indicated with thick lines.

1.3 (ACCESS1.3; Bi et al. 2013). ACCESS1.3 exhibits SW radiation errors in the high-latitude Southern Ocean during DJF typical of the persistent biases in CMIP3 and CMIP5 models. A first-order evaluation of ACCESS1.3 indicates SW cloud radiative effect (CRE_{SW}; the difference between outgoing fluxes at top of the atmosphere under clear-sky and cloudy-sky conditions) errors of 48 $W m^{-2}$ with respect to ISCCP flux data (ISCCP-FD) observations and 38 $W m^{-2}$ with respect to CERES synoptic 1° (SYN1deg) observations over the high-latitude Southern Ocean (Fig. 1); in the same region the bulk cloud errors include a 20% underestimate of total cloud cover (TCC) and a deficit of optically thick low and midtopped cloud (Fig. 2; see also Franklin et al. 2013a).

The purpose of this study is to develop an extended cloud regime methodology and to demonstrate its application to the evaluation of Southern Ocean cloud and radiation errors in ACCESS1.3. The satellite observations and reanalysis data used and the configuration of the GCM are described in section 2. The methodology for identifying hybrid cloud regimes is described in section 3, followed by the properties and statistics of the hybrid cloud regimes for ACCESS1.3, their contribution to the CRE_{SW} error, and their distribution in the context of a composite extratropical cyclone. To demonstrate the utility of the hybrid cloud regimes for making a quantitative and process-oriented assessment of the effects of changes to the model, we test some selected changes to

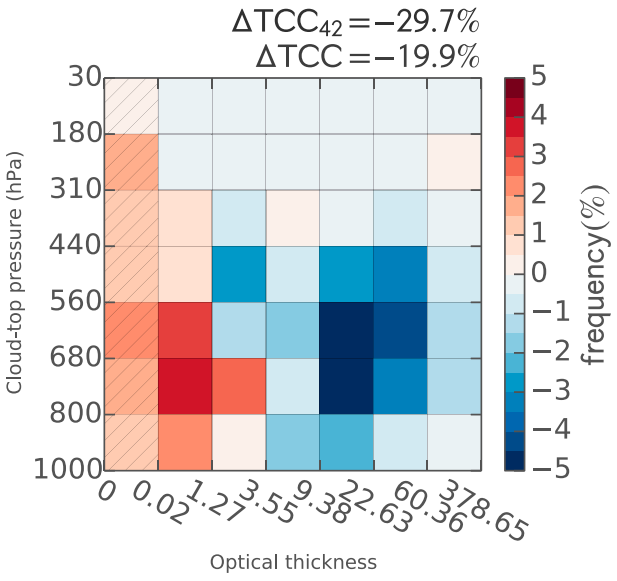

FIG. 2. The mean cloud bias (ACCESS1.3 − ISCCP) over the region of interest for two austral summers (DJF), presented as the difference between CTP-τ joint histograms. The part of the histogram representing subvisible optical thicknesses ($\tau < 0.3$), which is simulated in ACCESS1.3 but not observed in ISCCP, is hatched. At top-right the TCC error is indicated for the full joint histogram and for the visible (42 elements) joint histogram.

the model microphysics in section 4. The applications and limitations of the methodology for model evaluation are discussed in section 5, with some concluding remarks.

2. Data

a. Passive satellite observations

The International Satellite Cloud Climatology Project (ISCCP; Rossow and Schiffer 1999) combines passive observations from geostationary and polar-orbiting satellites to provide a continuous global dataset for the period July 1983–2009. Observations of cloud-top pressure (CTP) and cloud optical thickness (τ) are made at the scale of 1–5 km. The ISCCP D1 dataset consists of joint histograms of CTP-τ observations within a 280 km × 280 km equal-area grid at 3-h intervals in all day-lit areas. Upwelling top of the atmosphere (TOA) SW radiative flux observations are obtained from the ISCCP radiative flux profile dataset (ISCCP-FD; Zhang et al. 2005). Term CRE_{SW} is the difference between the upwelling TOA radiative fluxes under clear-sky and cloudy-sky conditions. The sign convention for TOA fluxes is such that the CRE_{SW} is negative (the cloud acts to reflect more SW radiation) and CRE_{LW} is positive (cloud inhibits LW radiation to space).

To quantify the observational uncertainty, we compare CRE_{SW} from ISCCP-FD against that from Clouds and the Earth's Radiant Energy System (CERES) gridded data (SYN1deg 3-h Ed3A; Wielicki et al. 1996), derived from the sun-synchronous *Aqua* and *Terra* satellites. The spatial patterns of the SW errors in ACCESS1.3 (Fig. 1) are qualitatively similar using the two observational datasets; the zonal means differ by about 10–15 W m^{-2} equatorward of 60°S but are very similar at high latitudes.

Two summers (2006–08; DJF) of daily averages of ISCCP D1 and TOA flux data were interpolated onto a regular 2.5° grid: the CTP-τ histograms were interpolated according to a nearest-neighbor interpolation scheme and radiative fluxes using linear interpolation. In keeping with previous studies (e.g., Haynes et al. 2011; Mason et al. 2014), daily averages of 3-h ISCCP observations are used.

b. Reanalysis

The European Centre for Medium-Range Weather Forecasts (ECMWF) interim reanalysis (ERA-Interim; Dee et al. 2011) is available at 1.5° spatial and 6-h temporal resolution. Two summers (2006–08; DJF) of ERA-Interim data were reinterpolated onto a regular 2.5° grid using a linear interpolation scheme. The first and second derivatives of the ERA-Interim mean sea level pressure (MSLP) were used to identify cyclone centers as described in Field and Wood (2007). Cyclone composites are constructed by reinterpolating contemporary data onto a regular 4000 km × 4000 km grid centered at the MSLP minimum of each identified extratropical cyclone.

c. Global climate model

ACCESS1.3 (Bi et al. 2013) is a coupled climate model developed by the Centre for Australian Weather and Climate Research (CAWCR). Its atmosphere model is based on the UKMO Unified Model (UM) Global Atmosphere model, version 1.0 (GA1.0; Hewitt et al. 2011). To facilitate the consistent comparison of simulated cloud with observations, the ISCCP satellite simulator (Klein and Jakob 1999; Webb et al. 2001), part of the Cloud Feedback Model Intercomparison Project (CFMIP) Observation Simulator Package (COSP; Bodas-Salcedo et al. 2008), is integrated into ACCESS1.3 (Franklin et al. 2013a). The ISCCP simulator output differs from ISCCP observations in that subvisible cloud ($\tau < 0.3$) are included; however, when comparing models to observations, these thin clouds are omitted, as it is assumed that they would not be detected by the ISCCP cloud detection algorithms (Klein and Jakob 1999; Webb et al. 2001).

ACCESS1.3 was run in atmosphere-only mode with prescribed sea surface temperatures at N96 resolution for two years (2006–08). The output fields were daily MSLP, TOA SW radiative fluxes for full-sky and clear-sky conditions, and CTP-τ joint histograms from the ISCCP simulator. These data were reinterpolated onto a 2.5° grid for consistency with satellite observations and reanalysis

data. MSLP and radiative fluxes were interpolated using a linear interpolation scheme, and ISCCP simulator data were interpolated using a nearest-neighbor interpolation scheme.

3. Evaluation of ACCESS1.3

a. Hybrid cloud regime methodology

In this section we extend the existing methodologies for assigning observed and simulated cloud properties to cloud regimes for model evaluation. Previous approaches have involved either clustering on the simulated cloud properties from a model (WT07)—so that the resultant cloud regimes accurately represent the model cloud behavior, but they are not necessarily comparable with observed cloud regimes—or assigning simulated clouds directly to predefined observed cloud regimes (WW09), maintaining a consistent set of cloud regimes against which GCMs can be evaluated, at the risk of not necessarily resolving the cloud structures peculiar to each model. Based on the strengths and weaknesses of the existing approaches, we aim to combine the advantages of both so that the extended cloud regime methodology is capable of resolving both the behavior of the GCM (i.e., the repeating structures of simulated cloud properties) and the cloud regimes identified in observational studies.

To achieve this, we cluster observed and simulated CTP-τ histograms simultaneously. The resulting clusters, which we call hybrid cloud regimes, represent a blend of model and observation: each cloud regime may consist of a mixture of observed and simulated clouds, or they may be made up of either mostly observed or mostly simulated clouds. It is worth considering what information we would expect the hybrid cloud regime approach to resolve in some idealized scenarios. If the GCM reproduces the observed cloud very accurately, then we could expect the resultant hybrid cloud regimes to be identical to the observed cloud regimes in terms of both physical characteristics (as represented by the average CTP-τ histogram of the cluster members) and geographic distribution. Conversely, if the GCM was unable to reproduce any cloud resembling the observations, then we would expect to identify a superset of independent cloud regimes populated either by observed or simulated clouds alone—that is, there would be no cloud regimes jointly populated by both. In practice we expect the results for a state-of-the-art GCM to lie somewhere between these two extremes: it is conceivable to identify certain observed cloud regimes that the model fails to reproduce and some simulated cloud regimes that do not occur in nature; we would also expect to identify jointly populated cloud regimes that the GCM can simulate in principle but which occur with the wrong frequency of occurrence or geographical distribution, or slight differences in cloud properties, and finally some cloud regimes that are well simulated in all respects. In the former cases, the cluster centroids would resemble those obtained from clustering observations and simulations independently; in the latter cases, we would find that the cluster centroid of the resulting hybrid cloud regimes are modified somewhat from the observed cloud regimes, reflecting the features of the simulated members. The advantages of having this comprehensive information and especially of using it to analyze model errors in other fields, such as cloud radiative effects, will become apparent when we apply this technique to the high-latitude Southern Ocean clouds below.

Using the method for identifying cloud regimes first described in Jakob and Tselioudis (2003), we apply the k-means clustering algorithm (Anderberg 1973) to the 42-element state vectors of the CTP-τ histograms from both the ISCCP observations and from the ISCCP simulator running in ACCESS1.3 (omitting the simulated $\tau < 0.3$ classes for consistency with observations), using 2 years of austral summer (DJF) data over the region of interest (50°–65°S). The pool of state vectors from which the hybrid cloud regimes are identified consists of equal parts observed and simulated cloud properties, which are not differentiated by the clustering algorithm. Consistent with Haynes et al. (2011) and Mason et al. (2014), clear conditions are not removed from the data before clustering, and instances of clear skies will be included in the hybrid cloud regime with the lowest total cloud cover. Because of the ubiquity of cloud in the Southern Ocean, completely clear skies at these scales are rare in both observations (0.3%) and the model (0.06%).

The clustering algorithm is somewhat subjective in that the number of clusters (k) must be specified. Rossow et al. (2005) propose four criteria by which k can be objectively chosen: 1) the stability of the resulting cluster centroids across random initializations of the algorithm, and for random subsets of the data; 2) avoiding similarity between cluster centroids; 3) avoiding similarity between the frequency of occurrence patterns of the clusters in space and time; and 4) ensuring the Euclidean distances between cluster centroids exceed the distances between cluster members. As Rossow et al. (2005) note, in practice criteria 1 and 4 are automatically met: the algorithm is restarted with randomly seeded centroids a number of times and the most stable solution is selected, and the algorithm iterates until the distance between cluster centroids is greater than the spread of cluster members.

Criteria 2 and 3 are intended to avoid redundant clusters. However, for the purposes of a hybrid cloud regime analysis—simultaneously clustering on two independent populations—this is not necessarily desirable: for

example, it is possible for a mostly simulated hybrid cloud regime to occur in a similar context—and therefore exhibit a similar spatial distribution—to a mostly observed cloud regime. As these cases provide information about the model errors, we would wish to resolve them.

Therefore, for the hybrid cloud regime analysis, we increase k until the set of clusters includes the observed cloud regimes identified previously. We note that the hybrid cloud regimes identified here are not identical to those identified for the broader Southern Ocean (30°–65°S; Haynes et al. 2011) and the refined analysis of midtopped cloud subregimes conducted for the high-latitude Southern Ocean (Mason et al. 2014), as the cloud regimes identified in the former study include lower-latitude clouds, and the cloud subregimes identified in the latter were derived by clustering within previously identified cloud regimes. Nevertheless, all of the features identified in the observational studies for the region of interest are represented in the hybrid cloud regimes.

For the area of interest in this study, two seasons (6 months) of data provide a large enough dataset that the hybrid cloud regimes are reliably identified. A test of robustness was made by clustering on randomly selected subsets of the data; the resulting cluster centroids were found to be substantially similar for even one month of data. We note that the relative frequencies of occurrence of the cloud regimes are more sensitive to interannual variability; we present these values here for evaluation of the GCM over the period in question, and not as a climatology of the identified cloud types.

Once the hybrid cloud regimes have been identified, each CTP-τ histogram (observed or simulated) is assigned to one of the cloud regimes. The assignation may be performed concurrent to the cloud regime identification, or subsequently. Assignation is determined by the least Euclidean distance between each CTP-τ joint histogram and the centroids of the cloud regimes. An alternative approach used in WW09 and subsequent studies calculates the least Euclidean distance between the total cloud cover (TCC; the sum of the joint histogram), mean cloud-top pressure ($\overline{\text{CTP}}$), and mean cloud albedo ($\overline{\alpha}$; derived from τ using the ISCCP lookup table reproduced in WW09). The WW09 methodology is intended for multimodel intercomparison, wherein the mean cloud properties are a simpler requirement for participating modeling centers and using the full CTP-τ joint histograms requires a greater volume of data output and computation. While the WW09 methodology produces coherent results in many studies, we note that the differences in cloud regime frequencies of occurrence when using the two assignation methods are not negligible, especially for cloud types with complex distributions of cloud-top properties. A comparison of the two methods using the observed cloud regimes of Haynes et al. (2011) and 5 years of ISCCP-D1 data between 30° and 65°S resulted in significant differences in the frequency of occurrence (>10%) of some cloud regimes (not shown). In the present application to a single GCM, it is practicable to use the full CTP-τ joint histograms in order to retain the structures of cloud-top properties, which are indicative of subgrid-scale variability in ISCCP observations (see discussion in Mace and Wrenn 2013; Mason et al. 2014).

b. *Identification and properties of hybrid cloud regimes*

Eleven hybrid cloud regimes (H1–H11, ranked from high to low CTP and from low to high τ) are found to be sufficient to represent the observed cloud regimes within the region of interest, as well as the emergent features of mostly simulated cloud regimes. The CTP-τ joint histograms represent the average of all observed and simulated members of each hybrid cloud regime (Fig. 3). It is helpful to make a coarse classification by CTP level, grouping the 11 hybrid cloud regimes into boundary layer, low, midtopped, and frontal cloud regimes. The three lowest hybrid cloud regimes (H1–H3) are predominantly boundary layer clouds representing shallow cumulus (H1) through to cumulus–stratocumulus transition clouds (H3). The low hybrid cloud regimes (H4 and H5) are associated with a range of marine stratiform clouds. The hybrid cloud regimes identified as midtopped (H6–H8) are consistent with Mason et al. (2014) and are dominated by low cloud (see also Haynes et al. 2011; Bodas-Salcedo et al. 2014) under a range of mostly subsiding conditions, as distinct from the shallow frontal cloud regime (H9; Mason et al. 2014). The frontal hybrid cloud regimes (H9–H11) also include prefrontal cirrus (H10) and deep frontal cloud (H11); we note that, while H9 occurs at a lower CTP level than the higher frontal cloud regimes H10 and H11, it is displayed between the latter in the figures to save space.

By assigning each daily CTP-τ histogram to a hybrid cloud regime, we derive the relative frequency of occurrence (RFO) of the hybrid cloud regimes over the region of interest during DJF in both the observations and ACCESS1.3, as an overall RFO (Table 1) and as geographical distributions (Fig. 4). The overall RFO of each cloud regime gives an initial indication of the hybrid cloud regimes that are accurately represented in ACCESS1.3 and those that are over and underproduced in the model. Shallow cumulus and very low cloud fraction scenes (H1) are strongly overproduced in the model, as are low optical thickness low and midlevels clouds (H4 and H6); with the exception of deep frontal and cirrus clouds, the model severely

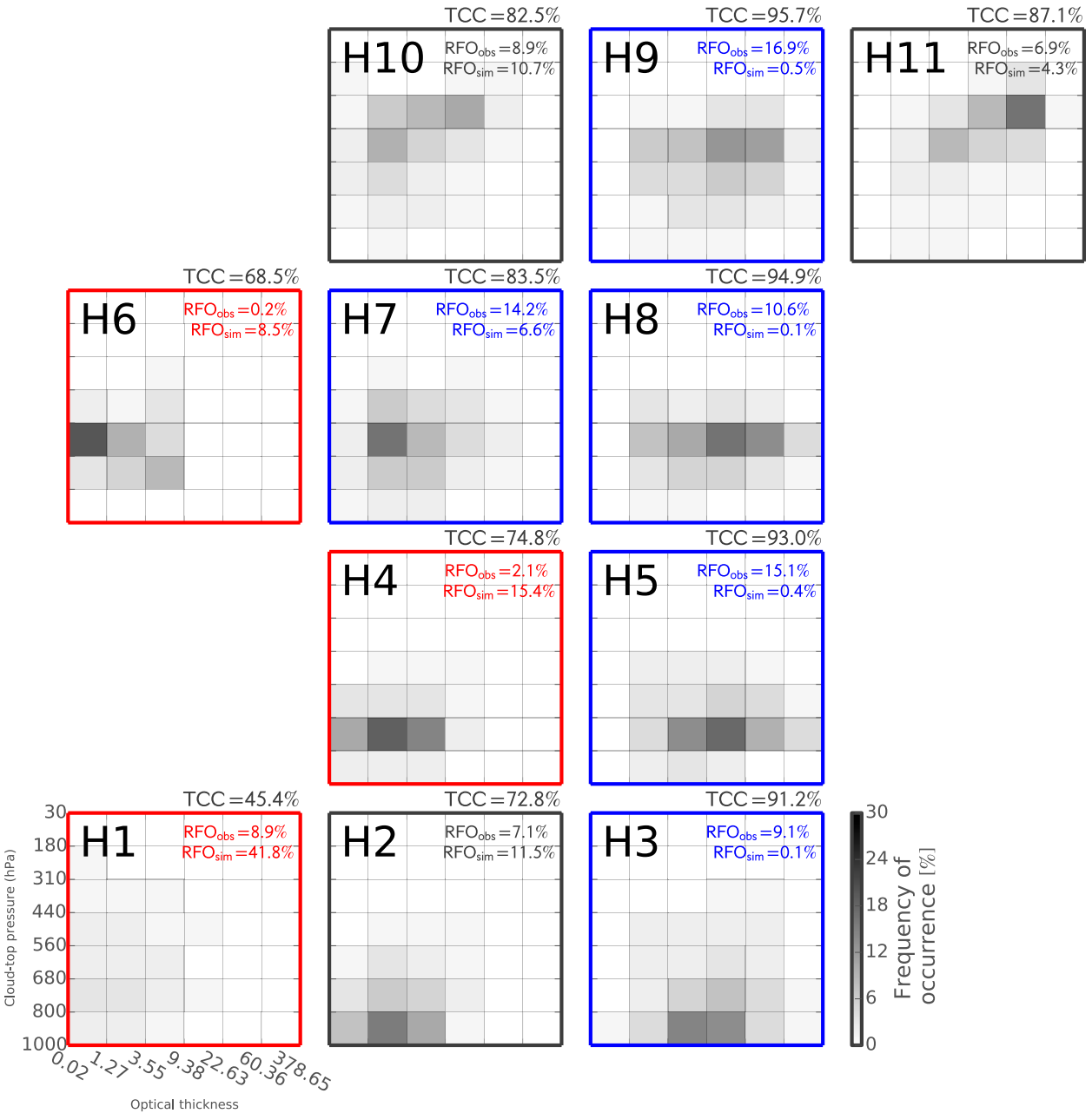

FIG. 3. The CTP-τ joint histograms representing the cluster centroids of the hybrid cloud regimes. The hybrid cloud regimes are arranged according to the dominant features of the joint histograms with the optically thinnest and lowest cloud regime in the bottom-left corner, and the optically thickest and highest cloud regime in the top-right corner, such that clouds of similar CTPs are comparably along the horizontal axis and similar optical thicknesses along the vertical axis. The mean observed and simulated RFO over the regions of interest are indicated in the top-right corner of each histogram. Where the cloud regime is underrepresented (underrepresented) in ACCESS1.3 by more than 50% with respect to the observed value, the histogram is bordered in blue (red). The TCC for each cloud regime (the sum of each joint histogram) is indicated at top right of each histogram.

underrepresents optically thick clouds at all levels (H3, H5, H8, and H9).

Cloud fractions are underestimated in ACCESS1.3 by 10%–20% for almost all cloud regimes, consistent with the overall deficit of TCC in the model. The tendency of the model to produce low cloud fractions is most apparent in the overproduction of the lowest cloud fraction, lowest optical thickness cloud regime (H1) throughout the area of interest (RFO of 42% compared with 9% observed). The CTP-τ histogram of H1 shows

TABLE 1. The observed (obs) and simulated (sim) properties of the hybrid cloud regimes.

CTP class	Cloud regime	TCC (%)		RFO (%)		CRE_{SW} ($W m^{-2}$)		
		Obs	Sim	Obs	Sim	Obs (ISCCP-FD)	Obs (CERES)	Sim
Boundary layer	H1	63.0	42.8	8.9	41.8	−76.8	−77.1	−88.0
	H2	74.6	71.6	7.1	11.5	−86.0	−81.0	−104.2
	H3	91.9	79.7	9.1	0.1	−149.6	−134.3	−124.4
Low	H4	85.5	72.6	2.1	15.4	−101.8	−99.1	−103.4
	H5	93.9	76.2	15.1	0.4	−154.8	−140.3	−120.9
	H6	89.7	66.4	0.2	8.5	−96.3	−99.8	−95.7
Midtopped	H7	89.5	73.6	14.2	6.6	−116.0	−113.6	−99.6
	H8	95.1	74.6	10.5	0.1	−159.8	−148.6	−111.5
	H9	96.4	76.5	16.9	0.5	−171.8	−158.8	−95.4
Frontal	H10	93.3	73.6	8.9	10.7	−140.1	−133.3	−87.4
	H11	97.2	75.0	6.9	4.3	−194.0	−178.2	−91.2

that this cloud regime includes low amounts of optically thin cloud from the surface to midlevels; we also note that the simulated spatial distribution of H1 is in areas associated not only with the observed boundary layer cloud regimes but also with the occurrence of the midtopped cloud regime H7 in the high-latitude Atlantic and Indian Oceans.

ACCESS1.3 has a systematic bias toward optically thin (low τ) low and midtopped cloud regimes. The low-τ errors appear to lead to H1 being simulated where H2 is observed (in the eastern edges of the Pacific and Indian Ocean basins), and the simulated distribution of H2 downstream of the Drake Passage resembles that observed of H3. A tendency to create low-τ counterparts of observed cloud regimes gives rise to the low and midtopped hybrid cloud regimes H4 and H6, respectively. H4 (predominantly simulated) and H5 (predominantly observed) differ in mean cloud-top properties but correspond very closely in terms of overall RFO (15%) and distribution in the high-latitude Atlantic and central Pacific oceans. Similarly, the optically thin midtopped cloud regime H6 is simulated in the high-latitude Atlantic and Pacific Oceans where H7 is observed. Corresponding to the overprediction of these low-τ cloud regimes in ACCESS1.3, the optically thickest low and midtopped hybrid cloud regimes are very rarely simulated.

The warm frontal cloud regime H9 is almost absent in ACCESS1.3, compared with an observed RFO of 16%, and has no clear compensating cloud regimes as identified above. As distinct from a systematic deficiency in cloud properties, this cloud error may be related to the representation of a dynamical process in the model. The higher frontal cloud regimes H10 and H11 are simulated with similar RFO to observations, but with a less cohesive distribution around the midlatitude storm track.

With an evaluation of the occurrence of the hybrid cloud regimes in the model and observations, the major cloud errors in the GCM are made explicit in a process-oriented way. The tendencies toward low TCC and low-τ cloud are manifest in the predominantly simulated low and midtopped hybrid cloud regimes (H4 and H6) and the overprediction of sparse cloud regime (H1). While the prefrontal cirrus (H10) and frontal (H11) hybrid cloud regimes are relatively wellrepresented in the GCM, the shallow frontal hybrid cloud regime (H9) is almost absent. We next turn our attention to quantifying how these cloud errors contribute to the overall SW radiation bias.

c. *Contributions to SW radiation bias*

Eleven hybrid cloud regimes have been identified from passive satellite observations and simulated cloud properties in ACCESS1.3. The most significant and recurring deviations from observed cloud properties give rise to hybrid cloud regimes that are not frequently found in the observations: these predominantly simulated hybrid cloud regimes provide an initial indication of the major cloud errors in the GCM. By associating the hybrid cloud regimes with radiation errors, we can quantify the relative contributions of these major cloud errors to the total SW cloud radiative effect bias in the high-latitude Southern Ocean in ACCESS1.3.

The cloud radiative effect (CRE) is the difference between clear-sky and cloudy-sky TOA radiative fluxes. Since outgoing fluxes at TOA are defined as positive and cloud typically has the effect of increasing reflected SW radiation, values of CRE_{SW} are negative. The hybrid cloud regimes with the lowest observed $\overline{CRE_{SW}}$ are generally those with the optically thickest clouds and the highest total cloud cover (Table 1); however, the spatial distribution of the cloud regime is also important. We note that the differences between CRE_{SW} with respect to ISCCP-FD and CERES observations are greatest for the optically thick cloud regimes (e.g., H3, H5, H8, H9, and H11), where the observational uncertainly is as much as $15 W m^{-2}$. We therefore include both observational datasets in what follows, but unless otherwise

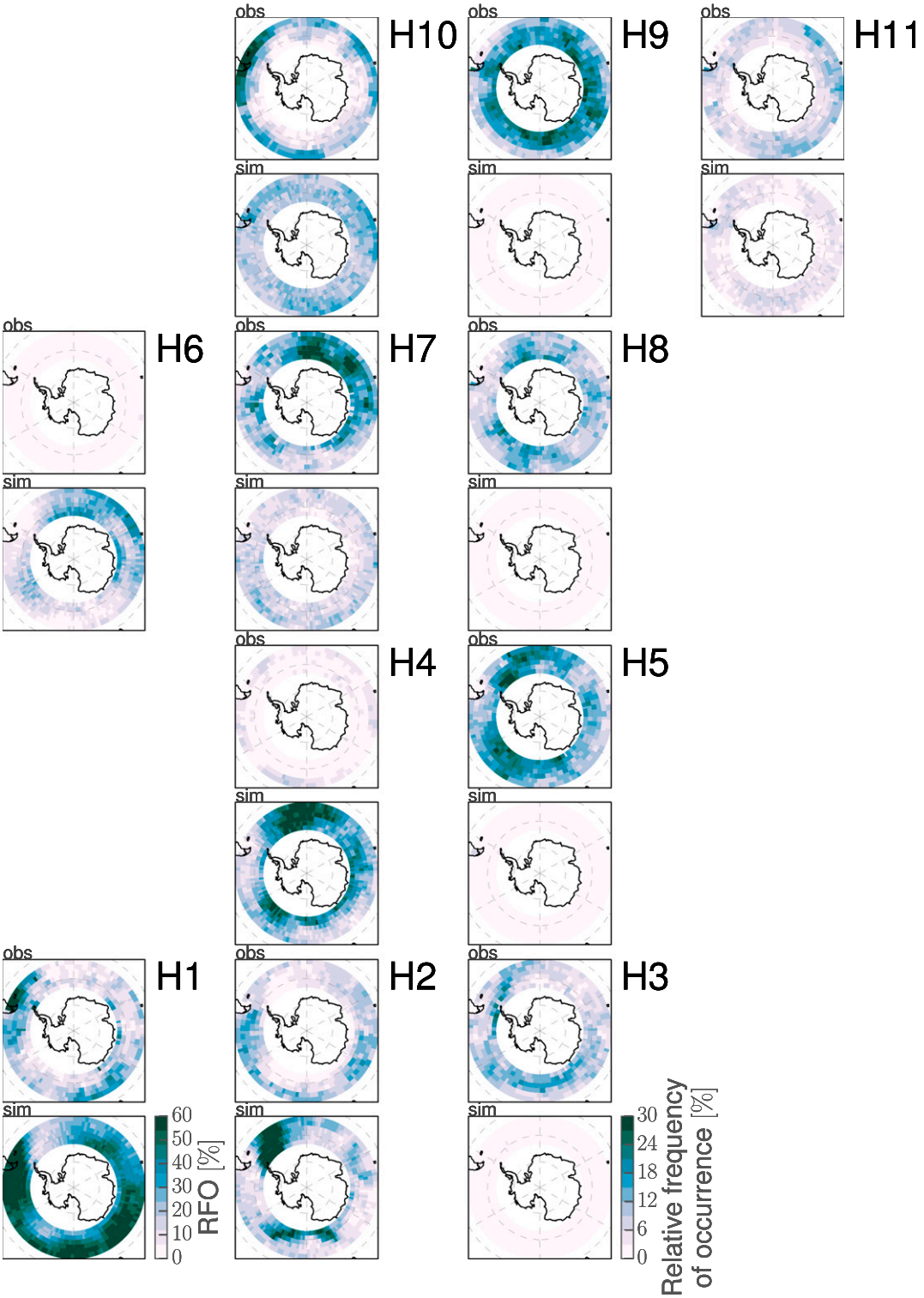

FIG. 4. Maps of the observed and simulated RFO of the hybrid cloud regimes over the region of interest. As in Fig. 3, the hybrid cloud regimes are arranged according to the dominant features of the CTP-τ histogram, with the optically thinnest and lowest regime in the bottom-left map and the optically thickest and highest cloud regime in the top-right map. Note that the simulated RFO of H1 is on a different color scale to resolve the significant overproduction of this hybrid cloud regime in ACCESS1.3.

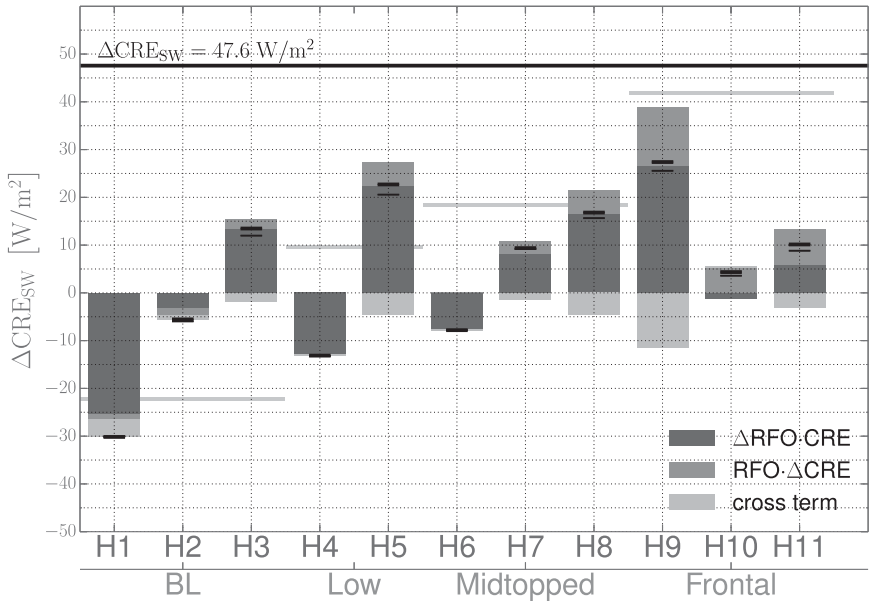

FIG. 5. The CRE_{SW} bias in ACCESS1.3 with respect to ISCCP-FD radiative flux observations. The biases are decomposed into parts related to errors in RFO and CRE_{SW}, and a cross term. Thick (thin) bars indicate the total CRE_{SW} bias associated with each cloud regime with respect to ISCCP-FD (CERES) observations, and the total mean bias over the region of interest is indicated with a thick black line. Pale bars indicate the net contribution to the CRE_{SW} error across each CTP-level class.

stated, the ΔCRE_{SW} is presented with respect to ISCCP-FD.

The mean SW cloud radiative effect bias (ΔCRE_{SW}) associated with each hybrid cloud regime is calculated by subtracting observed values of CRE_{SW} from the simulated values for the instances where each hybrid cloud regime is identified. Accordingly, positive ΔCRE_{SW} indicate insufficent—or insufficiently reflective—cloud in the model, and negative biases indicate too-cloudy or too-reflective cloud errors.

The total Southern Ocean DJF $\overline{\Delta CRE_{SW}}$ can be decomposed (following WT07) into parts corresponding to errors in the cloud regime frequency of occurrence or spatial distribution (RFO errors), errors in cloud regime radiative properties (CRE errors), and a cross term of covariant errors. The total bias is the sum of decomposed errors for all cloud regimes, such that

$$\overline{\Delta CRE_{SW}} = \sum_{r=1}^{n} \underbrace{CRE_{SWr} \cdot \Delta RFO_r}_{\text{RFO errors}} + \sum_{r=1}^{n} \underbrace{CRE_{SWr} \cdot \Delta RFO_r}_{\text{CRE errors}} + \sum_{r=1}^{n} \underbrace{CRE_{SWr} \cdot \Delta RFO_r}_{\text{cross term}}. \quad (1)$$

The decomposed ΔCRE_{SW} associated with each hybrid cloud regime (Fig. 5) is dominated by RFO-related errors; this is partially a consequence of the hybrid cloud regime methodology, in which simulated clouds that are sufficiently different in their cloud-top properties from observed clouds form new, predominantly simulated, clusters. This is especially true for the optically thin low and midtopped hybrid cloud regimes that are almost never observed (H4 and H6). In comparing the magnitude of ΔCRE_{SW} for ISCCP-FD and CERES observations, we note that the optically thickest cloud regimes exhibit lower errors with respect to CERES observations; as noted earlier, this corresponds to a total error of $38\,W\,m^{-2}$. To avoid redundancy in the following discussion, we refer to SW errors with respect to ISCCP-FD observations unless otherwise stated.

At each CTP level, the optically thinner cloud regimes make a small or negative contribution to the ΔCRE_{SW}, while the optically thick hybrid cloud regimes are associated with larger positive biases. This indicates that the low-τ, low-TCC hybrid cloud regimes—which occur with similar distributions to their high-τ counterparts—partially compensate for the latter. In the case of the low cloud regimes, the total error associated with the low-RFO and low CRE_{SW} of H5 ($23\,W\,m^{-2}$) is partially compensated by the high RFO of H4 ($-13\,W\,m^{-2}$); the net ΔCRE_{SW} related to low cloud is $10\,W\,m^{-2}$. Similarly,

the overprediction of the optically thinnest midtopped hybrid cloud regime H6 partially compensates ($-8\,\mathrm{W\,m^{-2}}$) for the low RFO of H7; the majority of the error associated with midtopped cloud ($18\,\mathrm{W\,m^{-2}}$) is related to the underprediction and low $\mathrm{CRE_{SW}}$ of the optically thicker H8.

The strongest compensating (negative) contribution to $\Delta\mathrm{CRE_{SW}}$ is associated with the low-TCC, low-τ hybrid cloud regime H1. Despite being associated with the lowest observed cloud fractions and cloud brightnesses, H1 contributes $-30\,\mathrm{W\,m^{-2}}$ to the net $\Delta\mathrm{CRE_{SW}}$. This is due to H1 accounting for more than 40% of the high-latitude Southern Ocean cloud in ACCESS1.3. The dominance of a low-TCC and low-τ cloud regime is symptomatic of the two key systematic biases identified in Franklin et al. (2013a).

The greatest positive contributor to the net $\Delta\mathrm{CRE_{SW}}$ is H9, the warm frontal cloud regime observed at high latitudes but hardly represented in ACCESS1.3. The deficit in the occurrence of this cloud regime is not compensated for by any optically thinner cloud regimes. The frontal cloud regimes H10 and H11 contribute around $15\,\mathrm{W\,m^{-2}}$ to the overall bias. Unlike the cloud regimes at other CTP levels, the largest portion of these biases are due to CRE-related errors; the RFO-related errors may be related to the tendency in ACCESS1.3 toward a less coherent band of frontal cloud at lower latitudes (Fig. 4).

d. *Dynamical contexts of the hybrid cloud regimes*

We have used hybrid cloud regimes to identify the major shortcomings in the simulation of clouds in the high-latitude Southern Ocean in ACCESS1.3 and have quantified their contributions to the SW radiation errors. It remains to investigate if the hybrid cloud regimes are associated with consistent dynamical and thermodynamical processes. In observational studies it is common to characterize cloud regimes by their contemporary meteorology derived from reanalyses (e.g., Gordon and Norris 2010; Haynes et al. 2011; Mason et al. 2014). This approach should be well suited to GCMs, wherein these fields are directly available; however, direct comparisons of dynamical fields in GCMs and reanalysis are frustrated by possible errors in model dynamics. An alternative approach is to consider cloud regimes in the context of a composite extratropical cyclone, the structure of which is both well understood in terms of observed dynamical and thermodynamical structure and well resolved by climate models (Catto et al. 2010). An evaluation of Southern Hemisphere extratropical cyclones in an earlier version of the ACCESS model, modified to use the same cloud scheme as ACCESS1.3 (Govekar et al. 2014), found that the circulation and dynamical variables were significantly weaker than in reanalyses and showed that the deficits of low cloud in this context are consistent with the broader evaluation of clouds in ACCESS1.3 (Franklin et al. 2013a) and in other models. Extratropical cyclones are the dominant synoptic-scale feature in the high-latitude Southern Ocean in terms of both cloud and precipitation (Bodas-Salcedo et al. 2014; Papritz et al. 2014), and cloud regimes have been used effectively to evaluate cloud in this context (e.g., Bodas-Salcedo et al. 2012, 2014). However, we note that not all dynamical contexts relevant to the high-latitude Southern Ocean are necessarily represented within the composite extratropical cyclone. The clouds associated with other features in the high-latitude Southern Ocean, such as anticyclones and mesoscale cyclones, are of considerable interest for model evaluation but are not considered here.

We identify extratropical cyclones in observations and simulations as described in Field and Wood (2007) using MSLP from ERA-Interim to identify cyclone centers contemporary to the satellite observations. Cloud regime occurrence and TOA radiative flux fields from observations and ACCESS1.3 are reinterpolated on to a $2000\,\mathrm{km} \times 2000\,\mathrm{km}$ grid centered at each MSLP minimum, and candidates are filtered to select only cyclones with centers from 50° to 65°S latitude.

The observed RFOs of the hybrid cloud regimes in the context of the composite cyclone (Fig. 6) agree well with other composite cyclone studies (e.g., Bodas-Salcedo et al. 2012, 2014), with some key differences. The most physically important difference is that the midtopped cloud regimes identified in this study are located in separate and coherent parts of the extratropical cyclone. This reinforces the distinction between optically thin and optically thick midtopped, and shallow frontal cloud regimes made in Mason et al. (2014). The profiles of dynamical and thermodynamical properties from reanalysis (not shown) are consistent with those presented in previous studies (e.g., Gordon and Norris 2010; Haynes et al. 2011; Mason et al. 2014). The fronts associated with the composite extratropical cyclone are characterized by the occurrence of the cirrus (H10) and deep frontal (H11) cloud regimes. H10 is observed farther from the cyclone center and appears to be associated with both prefrontal cirrus and other high and thin cloud in other contexts. H11 is found along the warm and cold fronts. H9 occurs predominantly near the cyclone center and into the cold sector, and resembles the warm conveyor belt (WCB) flow that overshoots the warm front; we note that a similar midtopped cloud subregime identified in Mason et al. (2014) was associated with conditions resembling that of the WCB. The warm sector is also associated with the shallow cloud regime H3. The cold sector of the extratropical cyclone consists of easterly flow ahead of the warm front turning equatorward behind the storm center, where it meets the descending dry sector. The cold sector

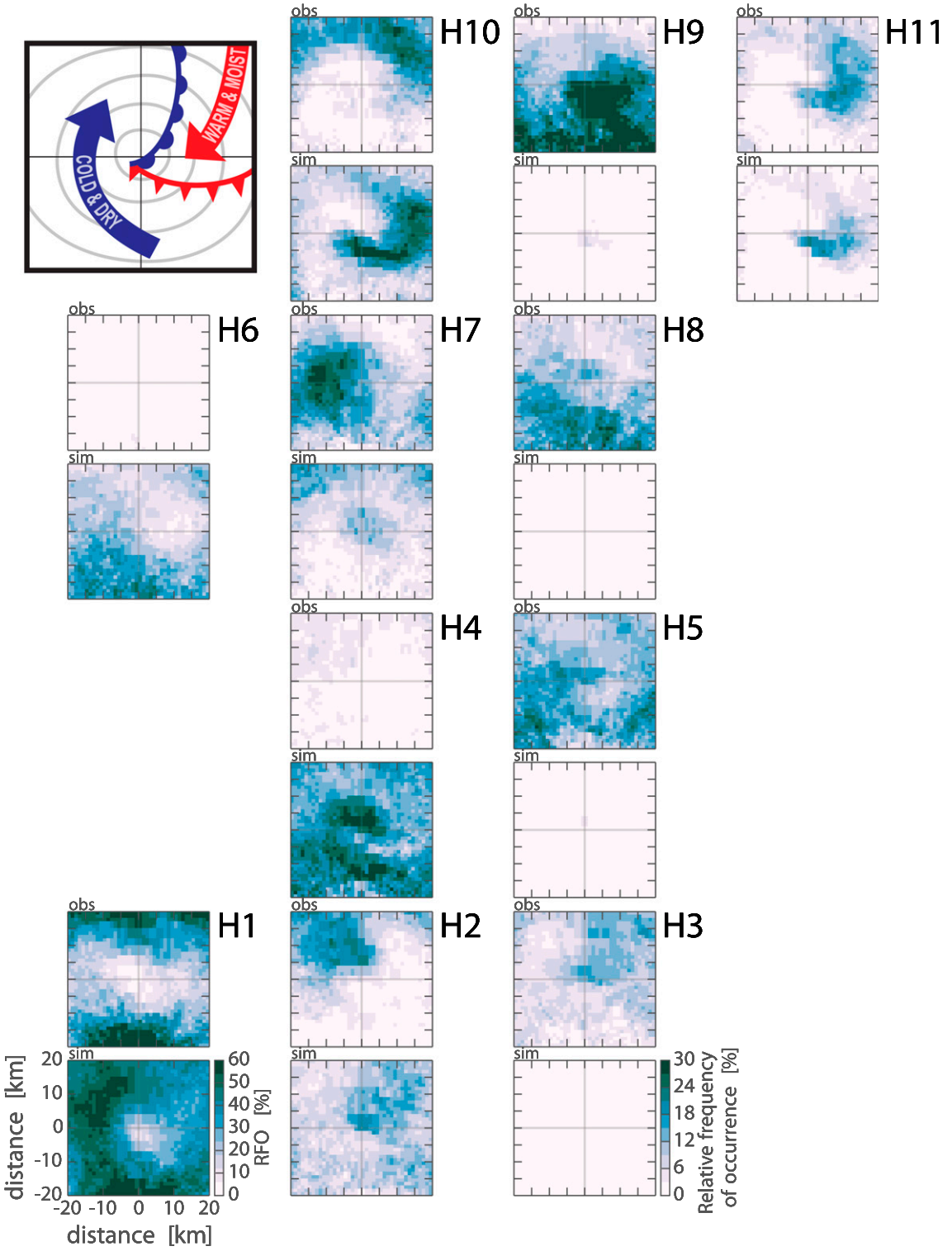

FIG. 6. Observed (above) and simulated (below) relative RFO of each hybrid cloud regime in the context of the composite extratropical cyclone. The cloud regimes are organized according to optical thickness (horizontal axis) and CTP (vertical axis). Note that the simulated RFO of H1 is on a different color scale to resolve the significant overproduction of this hybrid cloud regime in ACCESS1.3. A cartoon illustrating the orientation of warm and cold fronts and warm and cold sectors in Southern Hemisphere extratropical cyclones is shown at top left.

is dominated by low and midtopped stratiform cloud regimes H5 and H8, which form under subsiding conditions ahead of the warm front. These stratiform clouds transition to H7 in the postfrontal region of cold-air advection, and finally in the driest section the shallow cumulus (H2) dominates.

The ACCESS1.3 cloud errors in the context of the extratropical cyclone are consistent with those identified above. The frontal cloud regime H11 is found closest to the storm center: the shallow frontal cloud regime H9 is not present near the warm front, while the optically thinner H10 is found throughout the storm center and inner frontal region. The compensating relationships between predominantly simulated and predominantly observed hybrid cloud regimes are evident, indicating the consistent low-τ and low TCC biases. Where H3 is observed in the warm sector, its low-τ counterpart H2 is simulated. The cold sector is dominated by the low-τ and low-TCC biases, indicated by the overproduction of H1, H4, and H6.

The occurrence of the hybrid cloud regimes in the context of the extratropical cyclone illustrate consistent relationships between cloud properties and dynamical and thermodynamical conditions in both the observations and the model, reinforcing the corresponding spatial distributions of the mostly observed and mostly simulated hybrid cloud regimes over the high-latitude Southern Ocean. In both the composite cyclone and Southern Ocean maps, the significant overproduction of the low-TCC cloud regime H1 and the compensation of low-τ cloud regimes H2, H4, and H6 for their higher-τ counterparts are evident. These overpredicted optically thin low and midtopped cloud regimes make negative contributions to the SW radiation errors but only partially compensate for the lack of brighter clouds. This is consistent with the evaluation of GA2.0 and GA3.0 in Bodas-Salcedo et al. (2012), where the systematic bias toward optically thinner cloud led to the overassignation of shallow cumulus and cumulus–stratocumulus transition cloud regimes, especially in the cold-air section of extratropical cyclones. In the present study the use of hybrid cloud regimes permits many of these clouds to be assigned to distinct optically thinner stratocumulus and midtopped cloud regimes; nevertheless, the significant overproduction of H1 in this part of the extratropical cyclone is indicative of the magnitude of the cloud fraction and optical thickness errors in the model.

In contrast to the cloud regimes used in Bodas-Salcedo et al. (2012), wherein a single midtopped cloud regime was identified more than 30% of the time in both the cold-air sector and the warm front part of the composite extratropical cyclone, the distinction between shallow frontal (H9), optically thin (H7), and stratiform (H8) midtopped hybrid cloud regimes are confirmed by their distributions through the extratropical cyclone. The single largest contributor to the CRE_{SW} error is the near-absence of H9 in ACCESS1.3.

4. Evaluation of parameterization changes

We have used the hybrid cloud regimes to associate cloud and radiation errors in ACCESS1.3 in a process-oriented way. The identification of hybrid cloud regimes is a diagnostic of the simulated cloud properties in a GCM, making this approach suited to quantifying the sensitivity of the errors to changes made to the model. In this section we illustrate the use of the hybrid cloud regimes to evaluate the sensitivity of the radiation errors to targeted changes to cloud parameterizations in ACCESS1.3 and to quantify their effects on the hybrid cloud regimes.

ACCESS1.3 is characterized by systematic deficits of both TCC and τ affecting low and midtopped cloud in the high-latitude Southern Ocean. The low-τ bias suggests that errors in cloud properties relating to microphysical parameterizations may be affecting the cloud radiative effect. Relevant cloud properties include cloud thermodynamic phase, droplet size and concentration, and total cloud amount or cloud lifetime, which are affected by precipitation rates and mixing with dry air.

To target the optical thickness biases, we make three changes to the representation of clouds intended to reduce the Southern Ocean cloud and radiative biases in ACCESS1.3. A new autoconversion scheme (Franklin 2008) is implemented; it was shown by Franklin et al. (2013b) to increase the occurrence of optically thicker low clouds and to reduce the overestimate of drizzle in tropical boundary layer clouds. The fall speeds of the ice aggregate category are reduced by one-third; Franklin et al. (2013a) demonstrated that by reducing these fall speed, the occurrence of optically thicker low- and midlevel clouds in ACCESS1.3 was increased over the Southern Ocean. A change is also made to the erosion time-scale parameter that controls the rate at which the liquid cloud fraction is reduced by the mixing of cloudy air with drier environmental air. This parameter takes the value of $-4 \times 10^{-5}\,s^{-1}$ in the control version of ACCESS1.3 and is reduced by half in the modified cloud parameterizations experiment. While this change directly affects the cloud fraction, it also indirectly affects the microphysical processes by changing the in-cloud water contents that are used in the microphysical parameterizations, such as the autoconversion scheme. We note that the autoconversion, ice fall speed, and erosion rate are not the only possible microphysics changes that could be made in order to increase cloud brightness. Changes to ice particle size, ice deposition rate, and

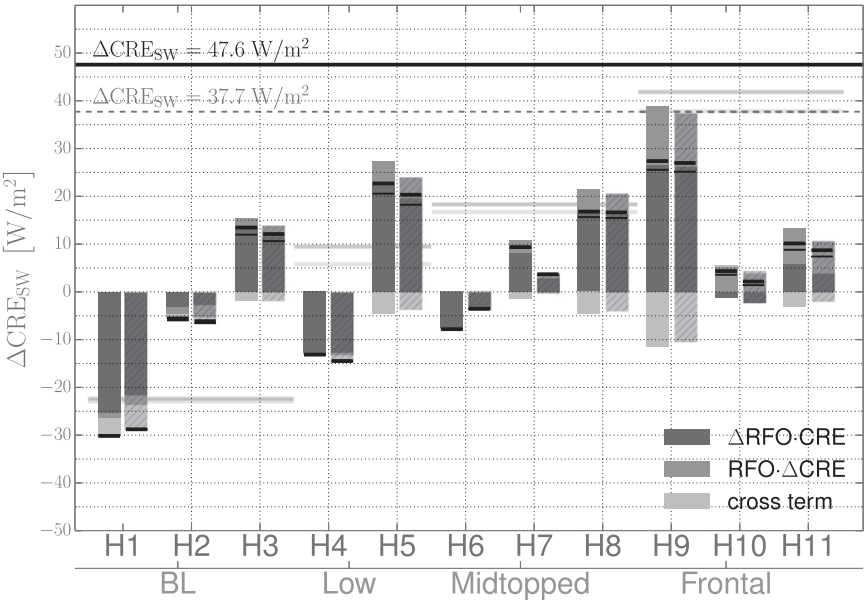

FIG. 7. As in Fig. 5, but comparing the control simulation (solid) against the modified microphysics case (hatched). Thick (thin) bars indicate the total CRE_{SW} bias associated with each cloud regime with respect to ISCCP-FD (CERES) observations. Pale and very pale bars indicate the combined contribution to the CRE_{SW} error across each CTP-level class in the original and modified cloud microphysics parameterizations.

heterogeneous nucleation temperature were also considered; the effects of the selected changes compare most favorably in a bulk evaluation of cloud properties against *CloudSat* and *Cloud–Aerosol Lidar and Infrared Pathfinder Satellite Observations* (*CALIPSO*) observations (not shown). Testing the three selected changes independently shows that the largest change in both the ISCCP diagnostics and CRE_{SW} comes from the different autoconversion scheme (not shown); the other two cloud microphysics changes also positively affect the radiative properties of the clouds over the Southern Ocean. The combination of the three changes produces the lowest Southern Ocean CRE_{SW} bias in ACCESS1.3 and is therefore used in this experiment. The positive effect of reducing drizzle rates and increasing cloud optical thickness by changing the autoconversion scheme and ice fall speed is consistent with the improved Southern Ocean CRE_{SW} biases between GA2.0 and GA3.0 shown in Bodas-Salcedo et al. (2012) and attributed to the introduction to the latter model of a prognostic rain formulation and a more accurate rain fall speed parameterization in GA3.0 (documented in Walters et al. 2011).

While our interest is in the sensitivity of the Southern Ocean cloud and radiation errors to these microphysics changes, their global impacts have also been investigated individually and in combination. Franklin et al. (2013b) showed that the Franklin (2008) autoconversion scheme led to more stratocumulus and less drizzle in the tropics, and an increase in stratocumulus and fair-weather cumulus cloud-top height attributed to a stronger cloud radiative effect driving enhanced entrainment at cloud top. Franklin et al. (2013a) showed that a reduction in ice fall speeds resulted in increased midlevel cloud fraction in the tropical warm pool and optically thicker high cloud. A reduction in the erosion rate leads to increased low- and midlevel liquid cloud fraction. The combined changes have a significant impact on the global DJF CRE_{SW} error with respect to ISCCP-FD observations, which is reduced from 5.7 $W m^{-2}$ for the control run to -2.6 $W m^{-2}$ with the modified microphysics.

ACCESS1.3 is run in atmosphere-only mode with the modified cloud microphysics in the same way as for the initial model evaluation. Two years of DJF data, including CTP-τ histograms from the ISCCP simulator, MSLP, and TOA radiative fluxes, are processed as described earlier. Instead of generating a new set of hybrid cloud regimes, the CTP-τ histograms are assigned to the cloud regimes derived from the standard ACCESS1.3 model; the differences in the RFO and CRE_{SW} can be compared directly, or summarized according to their contributions to the ΔCRE_{SW}.

The decomposed CRE_{SW} bias summarizes the effects of the modified microphysics on the radiation errors in ACCESS1.3 (Fig. 7). The total effect over the area of interest is a 10 $W m^{-2}$ reduction in the magnitude of the overall CRE_{SW} bias: approximately 20%–25% of the

total error with respect to ISCCP-FD and CERES observations. The majority of this improvement is due to a systematic increase of τ. The CRE_{SW}-related component of the error for each cloud regime decreases by as much as 2.0 W m^{-2}, including an increase in the magnitude of the negative errors associated with the optically thin hybrid cloud regimes (H1, H2, and H4), which act to compensate for the absent optically thicker cloud regimes.

Where the changes in the optical thickness of a cloud regime are large enough, instances of cloud previously belonging to one hybrid cloud regime may be assigned to an optically thicker hybrid cloud regime. These changes in cloud regime assignations lead to changes in the RFO-related error of both the prior and subsequent cloud regime: this is most apparent in the compensating RFO-related errors associated with the optically thin midtopped hybrid cloud regimes H6 and H7—each is reduced in magnitude by around 5 W m^{-2}, while the net bias associated with midtopped cloud overall is largely unchanged. The RFO of H1 decreases in a similar manner, corresponding to a 3 W m^{-2} improvement in the RFO-related bias—a net increase in the overall CRE_{SW} error, since H1 strongly compensates for the lack of optically thicker cloud regimes. Reductions of the errors associated with the frontal cloud regimes H10 and H11 are partly due to increased τ and partly due to increased RFO of both cloud regimes. This shift in cloud properties leads to reduced RFO of the optically thinnest cloud regimes (H1 and H6) and higher mean τ within cloud regimes, with the greatest net effect being a reduction of errors associated with low and frontal clouds of around 4 W m^{-2}. In several cases the increase in τ increased the magnitude of the compensating CRE_{SW} bias (H2 and H4), or it had little effect (H8 and H9).

The hybrid cloud regime approach allows us to resolve the contexts in which the changes to the microphysics had the most—and least—effect on the radiation errors. This evaluation illustrates the benefits of the methodology: major model errors can be explicitly identified, rather than assigned to an adjacent observed cloud regime. We can quantify how the model errors compensate for, or contribute to, the total radiation error, and we can evaluate changes to the model to determine whether an improvement to the total radiation error is the result of an increased compensating bias or from a shift toward the observed cloud state.

We reiterate that this experiment is intended to illustrate the use of the hybrid cloud regimes to evaluate model changes in a process-oriented way. The microphysics changes targeted the optical thickness biases in low and midtopped clouds, with the overall result of a 20%–25% improvement in the total Southern Ocean CRE_{SW} error, due to a brightening of low and midtopped clouds and an increased occurrence of high and frontal clouds. The largest single contributor to the radiation error, the shallow frontal cloud regime, which appears to be poorly simulated in ACCESS1.3, was not improved by these changes. It is likely that there are many other interrelated and unrelated contributors to the overall SW radiation errors in GCMs. For example, Bodas-Salcedo et al. (2012) evaluated modifications to the diagnosis of the shear-dominated boundary layer in GA3.0 (ACCESS1.3 is most similar to GA1.0), demonstrating a significant reduction in the CRE_{SW} bias related to enhanced production of stratocumulus cloud in the cold-air part of the composite extratropical cyclone, and concluded that further work was needed to increase the optical thickness of low and midtopped cloud regimes in the model.

5. Discussion and conclusions

We have presented a hybrid methodology for identifying cloud regimes from satellite observations and model-simulated cloud properties simultaneously. This approach expands on previous methodologies for identifying cloud regimes for model evaluation, with the advantage that the cloud regimes include a fixed reference to the observed cloud properties against which the models are evaluated, while also permitting cloud regimes that are peculiar to the model. The emergent hybrid cloud regimes include pairs of cloud regimes with similar spatial distributions and dynamical contexts, where one hybrid cloud regime is mostly simulated and the other is mostly observed; the differences between these pairs of hybrid cloud regimes relate to the major cloud errors in the GCM.

Based on two DJFs of simulated and observed cloud data, we identify 11 hybrid cloud regimes with which to evaluate high-latitude Southern Ocean clouds in ACCESS1.3. We use the cloud regimes to associate errors in cloud properties with SW radiation errors and to describe the dynamical context of the cloud regimes as inferred from composite extratropical cyclones.

Consistent with Franklin et al. (2013a), total cloud fraction in ACCESS1.3 is underpredicted, which contributes to the weak CRE_{SW} of most cloud regimes. The cloud regime associated with the lowest cloud fraction is overproduced in the model, especially in the cold and dry sectors of extratropical cyclones and throughout the high-latitude Southern Ocean; while the CRE_{SW} of this cloud regime is relatively weak, its strong overprediction has a significant compensating effect (-30 W m^{-2}) in the net SW bias.

Low τ biases in ACCESS1.3 were found across almost all cloud types. In some cases this is manifest in mostly simulated cloud regimes that are produced in place of optically thicker counterparts in observations, especially

in the cold and dry sectors of extratropical cyclones. These emergent cloud regimes partially compensate for optically thicker cloud regimes not well represented in the model. A combination of three microphysics changes targeting low cloud optical thickness were shown to mitigate the total SW radiation errors by 20%–25%. The result was a systematic increase in cloud brightness, which had the greatest net improvement on the CRE_{SW} of the low and frontal cloud regimes. Changes to the cloud microphysics to increase cloud optical thickness may constitute part of an improvement to the Southern Ocean cloud and radiation biases identified in ACCESS1.3, but in this case it was not sufficient to address some of the largest deficits in the optical thickness of stratiform clouds. This is consistent with the model evaluation of Bodas-Salcedo et al. (2012), who showed that improving the diagnosis of the shear-dominated boundary layer in a related GCM improved the simulation of stratocumulus cloud in the cold-air part of the composite extratropical cyclone but identified a need to further increase the optical thickness of low and midtopped cloud.

The largest contributor to the SW radiation bias over the Southern Ocean is the shallow frontal cloud regime observed at high latitudes and in the warm fronts of extratropical cyclones. These clouds were very rarely identified in the model, and a significant compensating relationship with an optically thinner cloud regime was not evident. The other frontal cloud regimes are also generally too optically thin: the cirrus cloud regime is simulated too frequently, especially close to the center of extratropical cyclones; and the frontal cloud regime is simulated infrequently and without the distinct midlatitude storm-track distribution found in observations. While the structure and frequency of Southern Ocean storms were sufficiently well represented in ACCESS1.3 to carry out a comparison of composite extratropical cyclones, we note that the significant errors in frontal cloud structure, especially relating to shallow frontal cloud at high latitudes, are consistent with the dynamically weak midlatitude storms identified in Govekar et al. (2014) for a related version of the ACCESS model. The insignificant impact on the shallow frontal cloud regime of the changes to the erosion rate and ice fall speeds—which could be expected to increase midlevel cloud fraction—suggests further work is required to evaluate the thermodynamics and dynamics of fronts.

We note that considering the Southern Ocean cloud regimes only in the context of extratropical cyclones is not necessarily representative. For example, while the shallow frontal cloud regime makes the largest net contribution to the SW bias, the warm front does not correspond to the region of greatest SW bias in the context of the composite extratropical cyclone—the cold-air advection in the cold and dry sectors (e.g., Bodas-Salcedo et al. 2012, 2014) where errors in total cloud cover and optical thickness dominate, and where modifications to the diagnosis of the shear-dominated boundary layer have had some success in mitigating the total error (Bodas-Salcedo et al. 2012). These two distinct dynamical contexts—cold-air advection and shallow frontal conditions—are each associated with midtopped cloud and are assigned to the same cloud regime in studies using WW09 cloud regime identification. We have demonstrated that the hybrid cloud regimes in this study are capable of distinguishing between midtopped cloud in these contexts, but further work is required to explore the representation of these distinct cloud processes: more detailed considerations of cold-air outbreaks and high-latitude storms may be an effective approach.

The approach of identifying pairs of mostly simulated and mostly observed hybrid cloud regimes has proved useful: the pairs were shown to be simulated with similar spatial distributions to their observed counterparts, and these relationships were also found in the dynamical context of a composite extratropical cyclone. However, more work is required to quantify the strength of the associations between these cloud regimes with dynamical contexts in the model and observations, perhaps by using the model in hindcast mode.

The hybrid cloud regimes have been identified for a single GCM, and this approach is not immediately suited to the evaluation of multiple models. However, the hybrid cloud regimes provide a fixed reference to cloud errors in the model, making this a promising tool for quantifying the effects of changes to the model on the properties and statistics in a process-oriented way.

While the Southern Ocean SW radiation errors in ACCESS1.3 are representative of radiation biases in many state-of-the-art GCMs, the nature and causes of these biases are almost certainly not the same in each model.

Acknowledgments. This research was supported by ARC Discovery and Linkage Grant Schemes (DP130100869 and LP0883961), and by the ARC Centre of Excellence for Climate System Science (CE110001028). We are grateful to Alejandro Bodas-Salcedo and Keith Williams at the UKMO for their generous cooperation and feedback.

REFERENCES

Anderberg, M. R., 1973: *Cluster Analysis for Applications.* Probability and Mathematical Statistics Series, Vol. 19, Academic Press, 359 pp.

Bi, D., and Coauthors, 2013: The ACCESS coupled model: Description, control climate and evaluation. *Aust. Meteor. Oceanogr. J.,* **63,** 41–64.

Bodas-Salcedo, A., M. J. Webb, M. E. Brooks, M. A. Ringer, K. D. Williams, S. F. Milton, and D. R. Wilson, 2008: Evaluating

cloud systems in the Met Office global forecast model using simulated CloudSat radar reflectivities. *J. Geophys. Res.,* **113,** D00A13, doi:10.1029/2007JD009620.

——, K. D. Williams, P. R. Field, and A. P. Lock, 2012: The surface downwelling solar radiation surplus over the Southern Ocean in the Met Office model: The role of midlatitude cyclone clouds. *J. Climate,* **25,** 7467–7486, doi:10.1175/JCLI-D-11-00702.1.

——, and Coauthors, 2014: Origins of the solar radiation biases over the Southern Ocean in CFMIP2 models. *J. Climate,* **27,** 41–56, doi:10.1175/JCLI-D-13-00169.1.

Bony, S., and J.-L. Dufresne, 2005: Marine boundary layer clouds at the heart of tropical cloud feedback uncertainties in climate models. *Geophys. Res. Lett.,* **32,** L20806, doi:10.1029/2005GL023851.

Catto, J. L., L. C. Shaffrey, and K. I. Hodges, 2010: Can climate models capture the structure of extratropical cyclones? *J. Climate,* **23,** 1621–1635, doi:10.1175/2009JCLI3318.1.

Cess, R. D., and Coauthors, 1990: Intercomparison and interpretation of climate feedback processes in 19 atmospheric general circulation models. *J. Geophys. Res.,* **95,** 16 601–16 615, doi:10.1029/JD095iD10p16601.

——, and Coauthors, 1996: Cloud feedback in atmospheric general circulation models: An update. *J. Geophys. Res.,* **101,** 12 791–12 794, doi:10.1029/96JD00822.

Colman, R., 2003: A comparison of climate feedbacks in general circulation models. *Climate Dyn.,* **20,** 865–873, doi:10.1007/s00382-003-0310-z.

Dee, D. P., and Coauthors, 2011: The ERA-Interim reanalysis: Configuration and performance of the data assimilation system. *Quart. J. Roy. Meteor. Soc.,* **137,** 553–597, doi:10.1002/qj.828.

Dufresne, J.-L., and S. Bony, 2008: An assessment of the primary sources of spread of global warming estimates from coupled atmosphere–ocean models. *J. Climate,* **21,** 5135–5144, doi:10.1175/2008JCLI2239.1.

Field, P. R., and R. Wood, 2007: Precipitation and cloud structure in midlatitude cyclones. *J. Climate,* **20,** 233–254, doi:10.1175/JCLI3998.1.

Franklin, C. N., 2008: A warm rain microphysics parameterization that includes the effect of turbulence. *J. Atmos. Sci.,* **65,** 1795–1816, doi:10.1175/2007JAS2556.1.

——, Z. Sun, D. Bi, M. Dix, H. Yan, and A. Bodas-Salcedo, 2013a: Evaluation of clouds in ACCESS using the satellite simulator package COSP: Global, seasonal, and regional cloud properties. *J. Geophys. Res. Atmos.,* **118,** 732–748, doi:10.1029/2012JD018469.

——, ——, ——, ——, ——, and ——, 2013b: Evaluation of clouds in ACCESS using the satellite simulator package COSP: Regime-sorted tropical cloud properties. *J. Geophys. Res. Atmos.,* **118,** 6663–6679, doi:10.1002/jgrd.50496.

Gates, W. L., and Coauthors, 1999: An overview of the results of the Atmospheric Model Intercomparison Project (AMIP I). *Bull. Amer. Meteor. Soc.,* **80,** 29–55, doi:10.1175/1520-0477(1999)080<0029:AOOTRO>2.0.CO;2.

Gordon, N., and J. Norris, 2010: Cluster analysis of midlatitude oceanic cloud regimes: Mean properties and temperature sensitivity. *Atmos. Chem. Phys.,* **10,** 6435–6459, doi:10.5194/acp-10-6435-2010.

Govekar, P. D., C. Jakob, and J. Catto, 2014: The relationship between clouds and dynamics in Southern Hemisphere extratropical cyclones in the real world and a climate model. *J. Geophys. Res. Atmos.,* **119,** 6609–6628, doi:10.1002/2013JD020699.

Haynes, J. M., C. Jakob, W. B. Rossow, G. Tselioudis, and J. Brown, 2011: Major characteristics of Southern Ocean cloud regimes and their effects on the energy budget. *J. Climate,* **24,** 5061–5080, doi:10.1175/2011JCLI4052.1.

Hewitt, H. T., D. Copsey, I. D. Culverwell, C. M. Harris, R. S. R. Hill, A. B. Keen, A. J. McLaren, and E. C. Hunke, 2011: Design and implementation of the infrastructure of HadGEM3: The next-generation Met Office climate modelling system. *Geosci. Model Dev.,* **4,** 223–253, doi:10.5194/gmd-4-223-2011.

Jakob, C., 2010: Accelerating progress in global atmospheric model development through improved parameterizations: Challenges, opportunities, and strategies. *Bull. Amer. Meteor. Soc.,* **91,** 869–875, doi:10.1175/2009BAMS2898.1.

——, and G. Tselioudis, 2003: Objective identification of cloud regimes in the tropical western Pacific. *Geophys. Res. Lett.,* **30,** 2082, doi:10.1029/2003GL018367.

——, ——, and T. Hume, 2005: The radiative, cloud, and thermodynamic properties of the major tropical western Pacific cloud regimes. *J. Climate,* **18,** 1203–1215, doi:10.1175/JCLI3326.1.

Klein, S. A., and C. Jakob, 1999: Validation and sensitivities of frontal clouds simulated by the ECMWF model. *Mon. Wea. Rev.,* **127,** 2514–2531, doi:10.1175/1520-0493(1999)127<2514:VASOFC>2.0.CO;2.

——, Y. Zhang, M. D. Zelinka, R. Pincus, J. Boyle, and P. J. Gleckler, 2013: Are climate model simulations of clouds improving? An evaluation using the ISCCP simulator. *J. Geophys. Res. Atmos.,* **118,** 1329–1342, doi:10.1002/jgrd.50141.

Li, J.-L. F., D. E. Waliser, G. Stephens, S. Lee, T. L'Ecuyer, S. Kato, N. Loeb, and H.-Y. Ma, 2013: Characterizing and understanding radiation budget biases in CMIP3/CMIP5 GCMs, contemporary GCM, and reanalysis. *J. Geophys. Res. Atmos.,* **118,** 8166–8184, doi:10.1002/jgrd.50378.

Mace, G. G., and F. J. Wrenn, 2013: Evaluation of the hydrometeor layers in the east and west Pacific within ISCCP cloud-top pressure–optical depth bins using merged *CloudSat* and CALIPSO data. *J. Climate,* **26,** 9429–9444, doi:10.1175/JCLI-D-12-00207.1.

Mason, S., C. Jakob, A. Protat, and J. Delanoë, 2014: Characterizing observed midtopped cloud regimes associated with Southern Ocean shortwave radiation biases. *J. Climate,* **27,** 6189–6203, doi:10.1175/JCLI-D-14-00139.1.

Oreopoulos, L., and W. B. Rossow, 2011: The cloud radiative effects of International Satellite Cloud Climatology Project weather states. *J. Geophys. Res.,* **116,** D12202, doi:10.1029/2010JD015472.

——, N. Cho, D. Lee, S. Kato, and G. J. Huffman, 2014: An examination of the nature of global MODIS cloud regimes. *J. Geophys. Res. Atmos.,* **119,** 8362–8383, doi:10.1002/2013JD021409.

Papritz, L., S. Pfahl, I. Rudeva, I. Simmonds, H. Sodemann, and H. Wernli, 2014: The role of extratropical cyclones and fronts for Southern Ocean freshwater fluxes. *J. Climate,* **27,** 6205–6224, doi:10.1175/JCLI-D-13-00409.1.

Rossow, W., and R. Schiffer, 1999: Advances in understanding clouds from ISCCP. *Bull. Amer. Meteor. Soc.,* **80,** 2261–2288, doi:10.1175/1520-0477(1999)080<2261:AIUCFI>2.0.CO;2.

——, G. Tselioudis, A. Polak, and C. Jakob, 2005: Tropical climate described as a distribution of weather states indicated by distinct mesoscale cloud property mixtures. *Geophys. Res. Lett.,* **32,** L21812, doi:10.1029/2005GL024584.

Stephens, G. L., 2005: Cloud feedbacks in the climate system: A critical review. *J. Climate,* **18,** 237–273, doi:10.1175/JCLI-3243.1.

Tan, J., C. Jakob, and T. P. Lane, 2013: On the identification of the large-scale properties of tropical convection using cloud regimes. *J. Climate,* **26,** 6618–6632, doi:10.1175/JCLI-D-12-00624.1.

Trenberth, K., and J. T. Fasullo, 2010: Simulation of present-day and twenty-first-century energy budgets of the southern oceans. *J. Climate,* **23,** 440–454, doi:10.1175/2009JCLI3152.1.

Tselioudis, G., W. Rossow, Y. Zhang, and D. Konsta, 2013: Global weather states and their properties from passive and active satellite cloud retrievals. *J. Climate,* **26,** 7734–7746, doi:10.1175/JCLI-D-13-00024.1.

Tsushima, Y., M. A. Ringer, M. J. Webb, and K. D. Williams, 2013: Quantitative evaluation of the seasonal variations in climate model cloud regimes. *Climate Dyn.,* **41,** 2679–2696, doi:10.1007/s00382-012-1609-4.

Walters, D. N., and Coauthors, 2011: The Met Office Unified Model Global Atmosphere 3.0/3.1 and JULES Global Land 3.0/3.1 configurations. *Geosci. Model Dev. Discuss.,* **4,** 1213–1271, doi:10.5194/gmdd-4-1213-2011.

Webb, M. J., C. Senior, S. Bony, and J.-J. Morcrette, 2001: Combining ERBE and ISCCP data to assess clouds in the Hadley Centre, ECMWF and LMD atmospheric climate models. *Climate Dyn.,* **17,** 905–922, doi:10.1007/s003820100157.

Wielicki, B. A., B. R. Barkstrom, and E. F. Harrison, 1996: Clouds and the Earth's Radiant Energy System (CERES): An Earth Observing System Experiment. *Bull. Amer. Meteor. Soc.,* **77,** 853–868, doi:10.1175/1520-0477(1996)077<0853:CATERE>2.0.CO;2.

Williams, K. D., and G. Tselioudis, 2007: GCM intercomparison of global cloud regimes: Present-day evaluation and climate change response. *Climate Dyn.,* **29,** 231–250, doi:10.1007/s00382-007-0232-2.

——, and M. J. Webb, 2009: A quantitative performance assessment of cloud regimes in climate models. *Climate Dyn.,* **33,** 141–157, doi:10.1007/s00382-008-0443-1.

Zhang, M. H., and Coauthors, 2005: Comparing clouds and their seasonal variations in 10 atmospheric general circulation models with satellite measurements. *J. Geophys. Res.,* **110,** D15S02, doi:10.1029/2004JD005021.